HNUE JOURNAL OF SCIENCE
Natural Sciences 2025, Volume 70, Issue 4, pp. 68-77
This paper is available online at http://hnuejs.edu.vn/ns
DOI: 10.18173/2354-1059.2025-0055

DENSITY FUNCTIONAL THEORY APPROACH IN INVESTIGATING STRUCTURAL AND ELECTRONIC PROPERTIES OF BISMUTH-BASED PHOTOCATALYSTS

Nguyen Huyen Nhung[1] and Tran Phan Thuy Linh[2,*]
[1]*Student of the Faculty of Physics, Hanoi National University of Education, Hanoi city, Vietnam.*
[2]*Faculty of Physics, Hanoi National University of Education, Hanoi city, Vietnam.*
[*]Corresponding author: Tran Phan Thuy Linh, e-mail: linhtpt@hnue.edu.vn

Received November 6, 2025. Revised December 18, 2025. Accepted December 30, 2025.

Abstract. Utilizing Density Functional Theory (DFT) as the computational method, we aimed to gain insights into the structural and electronic characteristics of Bi-based photocatalysts, particularly bismuth tungstate and bismuth molybdate. Both materials exhibit an orthorhombic structure and belong to the space group $Pca2_1$ under certain conditions. The exchange-correlation functional used throughout the study was the Perdew-Burke-Ernzerhof (PBE) functional within the generalized gradient approximation (GGA), enabling detailed analyses of their crystal structure, electronic band structure, density of states, and charge density. The electronic properties of both photocatalysts exhibit similar features as expected from the similarities in crystal structure. Notably, bismuth molybdate has a narrower band gap than bismuth tungstate, attributed to the atomic size difference between molybdenum and tungsten. The results confirm their semiconductor nature, highlighting their potential for sustainable-energy photocatalytic applications.

Keywords: DFT, Bismuth tungstate, Bismuth molybdate, photocatalyst, band gap.

1. Introduction

In recent decades, with the increasing demand for energy and the need to address environmental problems, different types of semiconductors have been researched due to their significant photocatalytic properties. Researchers have been striving to evaluate the intrinsic properties of the photocatalysts and enhance the efficiency using different techniques [1].

A narrow bandgap is observed in most bismuth-based photocatalysts due to the presence of Bi 6s and O 2p hybrid orbitals in the valence band, making them highly effective for visible light utilization. Over the past few years, a range of bismuth-based photocatalysts have been developed, progressing in the study of bismuth-based

nanomaterials for pollutant degradation and water splitting [2]. Despite their outstanding characteristics, such as good visible-light response, adjustable electronic band structure, and environmental friendliness, bismuth-based photocatalysts still perform inadequately in practical applications due to the high rate of recombination of the electron-hole pairs [3].

The two bismuth-based photocatalysts examined in this work are Bismuth tungstate (Bi_2WO_6), also known as BWO, and Bismuth molybdate (Bi_2MoO_6), known as BMoO. Both materials belong to the family of Aurivillius phases (n = 1 and 2) of the general formula $Bi_2A_{n-1}B_nO_{3n+1}$ (where A = Ca, Sr, Ba, Pb, Bi, Na, K and B = Ti, Nb, Ta, Mo, W, Fe) [4]. Under suitable synthesis conditions, they crystallize in the non-centrosymmetric orthorhombic space group $Pca2_1$, featuring two-fold screw axes along the c-direction and glide planes that govern atomic packing [5].

While Bi_2WO_6 is a promising material in electronic component manufacturing, its photocatalytic characteristics under visible light were first recognized for dioxygen production in water in 1999. Since then, Bi_2WO_6 has been extensively used to degrade different molecules under visible light [4].

Swapping W for Mo produces bismuth molybdate, which is widely utilized in solar cells, ionic conductors, catalysts, and other applications. Especially in the field of photocatalysis, Bi_2MoO_6 has been studied for its potential to address energy and environmental problems [6].

Throughout this study, we focus on investigating the crystal structure and electronic properties of two key bismuth-based photocatalysts, bismuth tungstate and bismuth molybdate. The DFT calculations were performed in the CASTEP module integrated into the Material Studio software.

2. Content

2.1. Computational method

The analysis of properties of the two materials is based on the calculation using the Density Functional Theory (DFT) approach, utilizing the CASTEP module. Convergence tests over various plane-wave cutoff energies and k-point meshes led us to adopt a cutoff energy of 590 eV and a 5×3×5 Monkhorst–Pack grid for geometry optimization of bismuth tungstate using valence configurations of Bi ($5d^{10}\ 6s^2\ 6p^3$), W ($5p^6\ 5d^4\ 6s^2$), and O ($2s^2\ 2p^4$). For bismuth molybdate, in which Mo ($4p^64d^5\ 5s^1$) replaces W, the corresponding value was 620 eV with the same 5×3×5 grid. Exchange–correlation effects were described by the Perdew–Burke–Ernzerhof (PBE) functional within the generalized gradient approximation (GGA). To maintain a reasonable accuracy while considering the computational cost, the pseudopotential was set to Ultrasoft. The self-consistent field (SCF) tolerance was set to 10^{-6} eV, indicating that the relaxation process iterates repeatedly until the total energy difference between successive steps falls below this threshold. Geometry optimizations were performed with convergence criteria of 0.03 eV/Å for maximum force, 0.05 GPa for stress, and 0.001 Å for displacement. These calculations considered scalar-relativistic effects while omitting spin–orbit coupling (SOC). The electronic properties, including the band structure, density of states, and charge density, were then analyzed based on the optimized structures.

2.2. Results and Discussion

2.2.1. Structural properties

The orthorhombic structures of the bismuth tungstate and bismuth molybdate consist of alternating $[Bi_2O_2]^{2+}$ sheets and layers of $[WO_6]^{2-}$ and $[MoO_6]^{2-}$ octahedral units, respectively, forming a stacked perovskite-like structure [3]. Table 1 and Table 2 present the calculated lattice parameters and the corresponding reference results for BWO and BMoO, respectively.

Table 1. Structural properties of Bi_2WO_6

Properties		**Present calculation**	**Previous theoretical results**	**Experimental results**
Cell angles		$\alpha = \beta = \gamma = 90°$		
Lattice constants (Å)	*a*	5.557	5.487 [7] 5.426 [8]	5.457 [9] 5.437[10]
	b	16.892	17.108 [7] 16.397 [8]	16.427 [9] 16.430 [10]
	c	5.607	5.518 [7] 5.426 [8]	5.436 [9] 5.458 [10]
Unit cell volume ($Å^3$)	V	526.36	517.93 [7] 483.73 [8]	487.29 [9] 487.21 [10]
Bond lengths (Å)	W-O	1.804 1.807 1.883 1.885 2.240 2.248	1.94 - 2.20 [7]	-
Bond angles	O-W-O	97.83° 98.74° 99.06° 101.22° 101.82° 153.43°	90°-180° [7]	-

The lattice constants of bismuth tungstate in the study deviate by 1% to 3% compared to theoretical calculations obtained using the GGA+U approach [7] and the PBE functional within GGA [8]. Similarly, when compared to experimental data [9], [10], the discrepancy remains around 2% to 3%. For the unit cell volume, the deviation is approximately 9%, notably large relative to previous studies. This can be explained by the omission of the SOC effect, which is significant for heavy atoms like Bi and W, and

may affect the equilibrium geometry. Additionally, the use of the GGA-PBE functional, which typically overestimates lattice parameters, also plays a role. Due to the distortion of the octahedral, the length of the bonds between W and O atoms varies in the range of 1.80 to 2.25 Å, while the angles of the bonds O-W-O exhibit a significant variability.

Table 2. Structural properties of Bi_2MoO_6

Properties		**Present calculation**	**Previous theoretical results**	**Experimental results**
Cell angles		$\alpha = \beta = \gamma = 90°$		
Lattice constants (Å)	*a*	5.482	5.51 [11] 5.50 [12]	5.506 [13] 5.51 [14]
	b	16.199	16.48 [11] 16.24 [12]	16.226 [13] 16.21 [14]
	c	5.509	5.53 [11] 5.49 [12]	5.487 [13] 5.49 [14]
Unit cell volume ($Å^3$)	V	489.23	502.15 [11] 490.37 [12]	490.21 [13] 490.35 [14]
Bond lengths (Å)	Mo-O	1.771 1.777 1.852 1.856 2.272 2.287	-	-
Bond angles	O-Mo-O	77.55° 79.22° 83.80° 101.95° 148.57° 171.72°	-	-

In the case of bismuth molybdate, the computed lattice constants show a deviation of below 1% with respect to those from the previous studies, both theoretical and experimental, which implies the reliability of the computational model in this work.

Owing to the similar Aurivillius-type layered perovskite structure, the properties of the two materials exhibit significant similarities in general. However, the size of Mo^{6+} is

smaller than that of W^{6+}, leading to smaller lattice constants, shorter length of the bond Mo – O (compared to that of W – O), as well as slightly different octahedral distortions.

2.2.2. Band structures

The band gaps obtained in the present calculation are listed in Tables 3 and 4 in comparison with reference results. Figure 1 and Figure 2 present the band structures of the two photocatalysts, with red and green lines drawn horizontally to mark the valence band maximum (VBM) and conduction band minimum (CBM).

Table 3. Calculated band gap of Bi_2WO_6 compared with references

Property	Present calculation	Previous theoretical results	Experimental results
Band gap (eV)	2.27	2.40 [14] (5.4%) 1.92 [7] (28%)	2.61 [15] (13%) 2.80 [16] (19%)

The calculated bandgap in this study is 2.27 eV, 5.4% lower than the previous theoretical result [14], which uses GGA-PBE with GW correlation and 18% higher than that in the work using the GGA+U approach [7]. Compared to the experimental data, a deviation of up to 19% is shown. This can be explained by the fact that the GGA approach tends to underestimate the band gap of materials, especially for the transition-metal oxides, which has been observed in a range of works before [17].

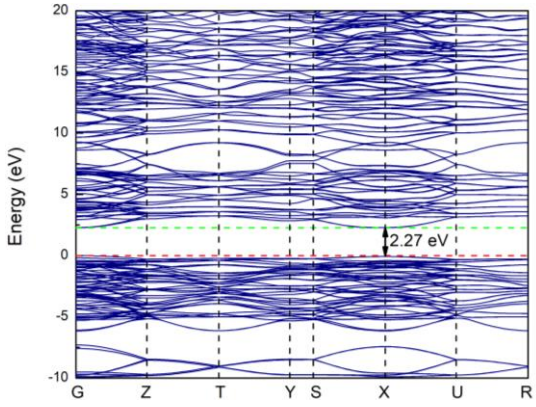

Figure 1. Band diagram structure of Bi_2WO_6

The band structure diagram indicates that both the VBM and CBM are located at the X point, exhibiting the direct nature of the band gap of bismuth tungstate.

Table 4. Calculated band gap of Bi_2MoO_6 compared with references

Property	Present calculation	Previous theoretical results	Experimental results
Band gap (eV)	1.89	1.76 [18] (7.4%) 2.44 [19] (23%)	2.59 [20] (27%) 2.60 [21] (27%)

The computed band gap of Bi_2MoO_6 shows a significant deviation of up to 27% relative to experimental results. The present calculation offers an improvement over the previous theoretical computation using GGA PBE (reference [18]), though it remains

23% lower than other values obtained using the same functional (reference [19]). A stronger tendency to underestimate the band gap is observed in the case of Bi_2MoO_6.

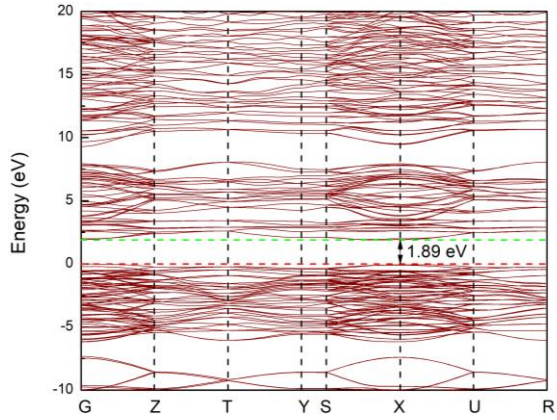

Figure 2. Band diagram structure of Bi_2MoO_6

The band structure diagram reveals that both the VBM and CBM are located at the k-point X, affirming a direct band gap for bismuth molybdate.

Bismuth molybdate and bismuth tungstate exhibit a direct band gap, facilitating efficient charge carrier transitions. However, due to structural differences, Bi_2MoO_6 has a smaller band gap, influencing its electronic and optical properties.

2.2.3. Densities of states

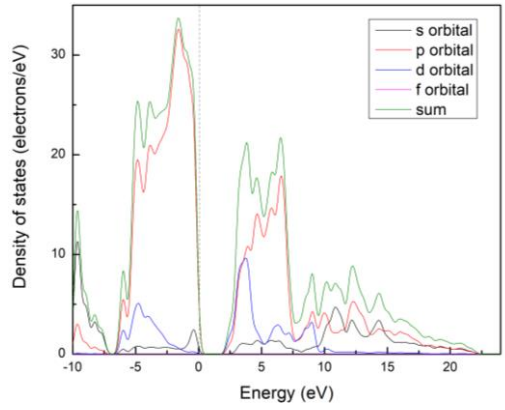

Figure 3. Orbital-resolved DOS of Bi_2WO_6

In Figures 3 and 5, the graph shows the partial density of states of BWO, highlighting the contributions from different orbitals, while Figures 4 and 6 show the projected density of states for the individual atomic species.

The total density of states shows the highest peak located between -2 and -1 eV, indicating occupied electronic states essential for bonding interactions. Specifically, the s orbital (represented by the black curve) exhibits minimal contribution across the energy range. The p orbital (red line) exhibits a large contribution to the total electronic states throughout, with significant peaks around -2 eV and 7 eV. The d orbital (blue line) contributes notably around 4 eV, strongly influencing conduction band transitions.

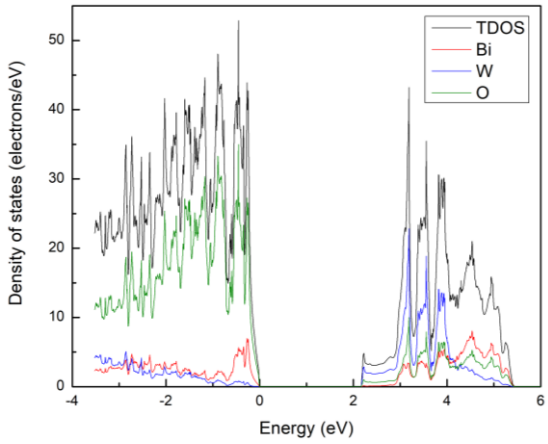

Figure 4. Atom-projected DOS of Bi_2WO_6

In the valence band region, the density of states is dominated by O 2p states, as indicated by the large contribution of the green curve, while Bi and W contributed comparatively less in this energy range. This suggests that the top of the valence band (VBM) is primarily composed of O 2p orbitals, which is typical for oxide-based photocatalysts. In contrast, the conduction band region shows a strong contribution from W 5d states, as illustrated by the prominent blue curve. Bi states contribute more notably in this region.

For Bi_2MoO_6, the peaks of the total density of state are around -2 eV, 3 eV, and 7 eV. In particular, similar to bismuth tungstate, the s orbital shows a modest contribution while the p orbital plays the dominant role in contributing to the overall electronic states in the considered energy range, especially in the valence band region. The d orbital has a peak around 3 eV, exerting a notable influence on the conduction band region.

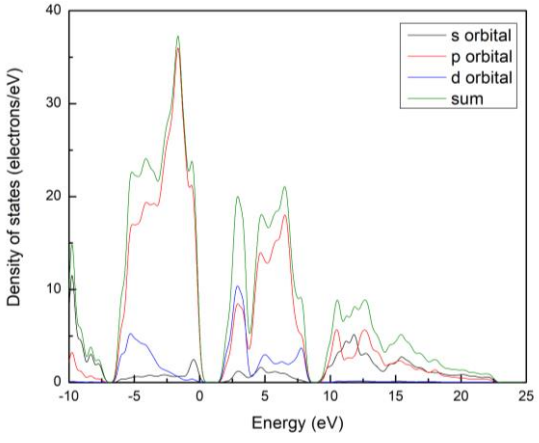

Figure 5. Orbital-resolved DOS of Bi_2MoO_6

The atomic-projected DOS of bismuth molybdate closely resembles that of bismuth tungstate. O 2p states also play the primary role in contributing to the TDOS in the valence band region. Moreover, Mo is observed to contribute modestly over this energy range. The prominent blue DOS peak near the CBM illustrates a dominant contribution of Mo 4d states in the conduction band region.

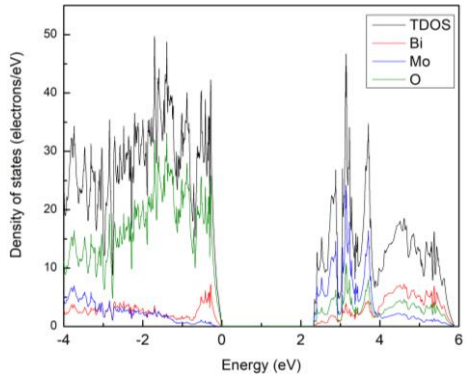

Figure 6. Atom-projected DOS of Bi_2MoO_6

Overall, the DOS of the two considered materials shows many similarities in the contribution of different orbitals and species to the total density of states, as reflected in the comparable patterns in their DOS plots.

2.2.4. Electronic charge densities

The charge density plots of the two materials are presented in Figures 7 and 8. The color scale ranges from blue, which illustrates low-density regions, to white, corresponding to intermediate-density regions, and to red, for high-density regions.

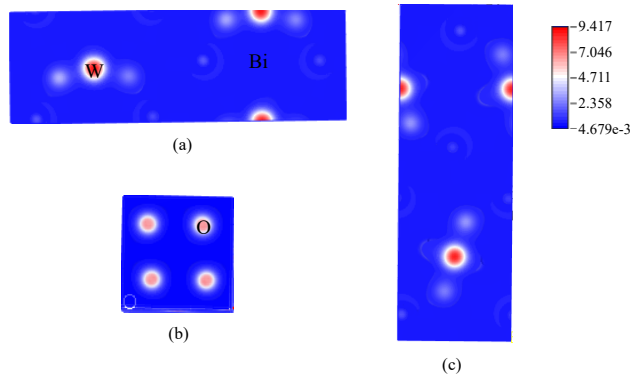

Figure 7. Electron density distribution of Bi_2WO_6 shown from different perspectives along the a, b, and c axes

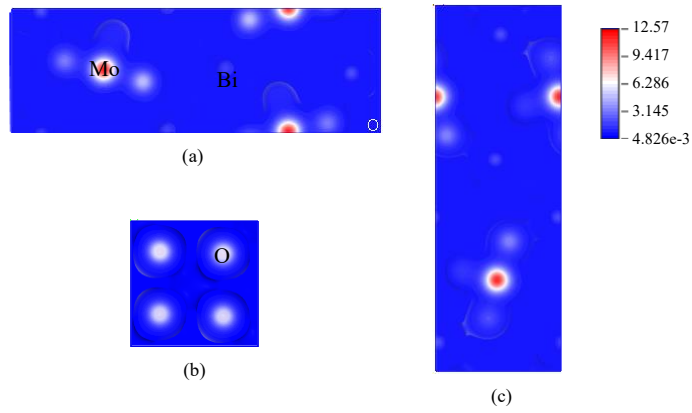

Figure 8. Electron density distribution of Bi_2MoO_6 shown from different perspectives along the a, b, and c axes

In the diagram of Bi_2WO_6, the most intense red spots highlight regions around W atoms, indicating strong electron localization in these areas. With the unequal distribution of the shared electrons between the two atoms, the W–O bonds are expected to display polar covalent interactions, which play a significant role in shaping both the band gap and optical properties.

The electronic charge density distribution of Bi_2MoO_6 closely resembles that of Bi_2WO_6, with the highest charge density concentrated around the Mo atoms. Less pronounced but still significant electron localization can be observed around O atoms. Therefore, the Mo–O bonds are expected to exhibit polar covalent interactions.

3. Conclusions

The optimized structures of Bi_2WO_6 and Bi_2MoO_6, obtained using the GGA PBE functional, align well with previous experimental and theoretical data, validating the computational approach. Both photocatalysts demonstrate semiconductor behavior, with direct band gaps of 2.27 eV for Bi_2WO_6 and 1.89 eV for Bi_2MoO_6. The difference in the band gaps is attributed to structural differences, particularly the size variation between W and Mo atoms. Regarding the density of states, the p orbital shows dominance in general, especially the O 2p states, which contribute dominantly to the valence band, while the s orbital only contributes modestly. The d orbital (W 5d and Mo 4d) influences notably in the conduction band region. The charge density distributions predict W–O and Mo–O bonds to display polar covalent interactions.

In future work, we propose investigating efficient doping strategies to enhance the performance of bismuth-based photocatalysts, particularly Bi_2WO_6 and Bi_2MoO_6.

Acknowledgments. This research was funded by the Ministry of Education and Training of Vietnam (MOET) under grant number B2024-SPH-16.

REFERENCES

[1] Ameta R & Ameta SC, (2016). *Photocatalysis: Principles and Applications* (1st ed.). CRC Press, p. 1-5.

[2] Pan Q, Wu Y, Su X, Yin Y, Shi S, Oderinde O, Yui G, Zhang C & Zhang Y, (2023). A review on the recent development of bismuth-based catalysts for CO_2 photoreduction. *Journal of Molecular Structure*, 1294(1), 136404.

[3] Zhang L, Li Y, Li Q, Fan J, Carabineiro S A C & Lv K, (2021). Recent advances on Bismuth-based photocatalysts: Strategies and mechanisms. *Chemical Engineering Journal*, 419, 129484.

[4] Elaouni A, El Ouardi M, BaQais A, Arab M, Saadi M & Ait Ahsaine H, (2023). Bismuth tungstate Bi_2WO_6: A review on structural, photophysical, and photocatalytic properties. *RSC Advances*, 13, 17476-17494.

[5] Ewald PP (Ed.), (1962). *Fifty years of X-ray diffraction*. International Union of Crystallography.

[6] Le MT, (2018). Bismuth molybdate-based catalysts for selective oxidation of hydrocarbons. *IntechOpen.* DOI: 10.5772/intechopen.75105.

[7] Materials Project, (2020). mp-23480: Bi_2WO_6 (orthorhombic, $Pca2_1$, 29). https://legacy.materialsproject.org/materials/mp-23480.

[8] Ahmad H, Rauf A, Ahmad A, Ata Ulhaq & Muhammad S, (2021). First-principles study on the electronic and optical properties of Bi_2WO_6. *RSC Advances*, 11(51), 32330-32338.

[9] Zeng T, Yu X, Hui S, Zhou Z & Dong X, (2015). Structural and electrical properties of Bi_2WO_6 piezoceramics prepared by solid state reaction method. *Materials Research Bulletin*, 68, 271-275.

[10] Knight KS, (1992), Mineralogical Magazine, 56, 399-409.

[11] Phuruangrat A, Putdum S, Dumrongrojthanath P, Thongtem S & Thongtem T, (2015). Hydrothermal synthesis of Bi_2MoO_6 visible-light-driven photocatalyst. *Journal of Nanomaterials*, 1-6. http://dx.doi.org/10.1155/2015/135735.

[12] Autes G, (2025). *Bi_2MoO_6 ICSD 37251*. https://www.materialscloud.org.

[13] SpringerMaterials, (2024). *Bi_2MoO_6 ($MoBi_2O_6$ rt) Crystal Structure.* https://materials.springer.com/isp/crystallographic/docs/sd_0306723.

[14] Chen P, Du T, Jia H, Zhou L, Yue Q, Wang H & Wang Y, (2022). A novel Bi_2WO_6/Si heterostructure photocatalyst with a Fermi level shift in the valence band realizes efficient reduction of CO_2 under visible light. *Applied Surface Science*, 585, 152665.

[15] Hossain Q S, Mahi T A, Nishat S S, Ahmed S, Sultana M, Khan M N I, Das H N, Bashar M S, Chowdhury F, Akhtar U S, Jahan S, Hossain K S & Ahmed I (2023). First-Principles Calculations on Electronic, Optical, and Phonon Properties of γ-Bi_2MoO_6. *RSC Advances*, 9(34), 36314-36325.

[16] Liu X, Gu S, Zhao Y, Zhou G & Li W, (2020). $BiVO_4$, Bi_2WO_6, and Bi_2MoO_6 photocatalysis: A brief review. *Journal of Materials Science & Technology*, 56, 45-68.

[17] Tian J, Sang Y, Yu G, Jiang H, Mu X, & Liu H, (2013). A Bi_2WO_6-Based Hybrid Photocatalyst with Broad Spectrum Photocatalytic Properties under UV, Visible, and Near-Infrared Irradiation. *Advanced Materials*, 25, 5075.

[18] Jing T, Dai Y, Wei W, Ma X, Huang B, (2014). Near-Infrared Photocatalytic Activity Induced by Intrinsic Defects in Bi_2MO_6 (M = W, Mo). *Physical Chemistry Chemical Physics*, 16, 18596-1860.

[19] Zhang B, Liu G, Shi H, Wu Q, Xue S, Shao T, Zhang F & Liu X, (2023). Density functional theory study of electronic structure and optical properties of Ln^{3+}-doped γ-Bi_2MoO_6 (Ln = Gd, Ho, Yb). *Crystals*, 13(1158).

[20] Guo C, Xu J, Wang S, Li L, Zhang Y & Li X, (2012). Facile synthesis and photocatalytic application of hierarchical mesoporous Bi_2MoO_6 nanosheet-based microspheres. *CrystEngComm*, 14(10), 3602.

[21] Umapathy V, Manikandan A, Arul Antony S, Ramu P & Neeraja P, (2015). Structure, morphology, and opto-magnetic properties of Bi_2MoO_6 nano-photocatalyst synthesized by the sol-gel method. *Transactions of Nonferrous Metals Society of China*, 25(10), 3271-3278.